fibers

MDPI

Article

Isolation and Properties of Cellulose Nanocrystals Fabricated by Ammonium Persulfate Oxidation from *Sansevieria trifasciata* Fibers

Nafiis Lazuardi Indirasetyo and Kusmono *

Department of Mechanical and Industrial Engineering, Faculty of Engineering, Universitas Gadjah Mada, Jln. Grafika No. 2, Yogyakarta 55281, Indonesia; n.lazuardi@mail.ugm.ac.id
* Correspondence: kusmono@ugm.ac.id; Tel.: +62-274-521-673

Abstract: Cellulose nanocrystals (CNCs) were successfully prepared from *Sansevieria trifasciata* fibers (STFs) via ammonium persulfate (APS) oxidation in this study. The influences of the APS concentration (1.1, 1.5, and 1.9 M) and oxidation temperature (60, 70, and 80 °C) on the characteristics of CNCs were studied. The resulting CNCs were characterized using Fourier transform infrared spectroscopy (FT-IR), X-ray diffraction (XRD), transmission electron microscopy (TEM), and thermogravimetric analysis (TGA). The TEM observations revealed that the rod-like CNCs possessed average length and diameter ranges of 96 to 211 nm and 5 to 13 nm, respectively, which led to an aspect ratio range of 16–19. The optimum conditions for maximum crystallinity were achieved at an oxidation temperature of 70 °C, a reaction time of 16 h, and an APS concentration of 1.5 M. All CNCs exhibited lower thermal stability compared to the STFs. The CNCs could be produced from the STFs through the APS oxidation process and showed potential as nanocomposite reinforcement materials.

Keywords: *Sansevieria trifasciata* fibers; cellulose nanocrystals; ammonium persulfate; oxidation

check for updates

Citation: Indirasetyo, N.L.; Kusmono. Isolation and Properties of Cellulose Nanocrystals Fabricated by Ammonium Persulfate Oxidation from *Sansevieria trifasciata* Fibers. *Fibers* **2022**, *10*, 61. https://doi.org/10.3390/fib10070061

Academic Editors: Jungmok You and Jeonghun Kim

Received: 31 May 2022
Accepted: 28 June 2022
Published: 13 July 2022

Publisher's Note: MDPI stays neutral with regard to jurisdictional claims in published maps and institutional affiliations.

Copyright: © 2022 by the authors. Licensee MDPI, Basel, Switzerland. This article is an open access article distributed under the terms and conditions of the Creative Commons Attribution (CC BY) license (https://creativecommons.org/licenses/by/4.0/).

1. Introduction

Sansevieria is a genus of flowering plants native to Indonesia, India, and Africa. Globally, there are more than twelve species present on different continents [1]. The most common species of sansevieria are *Sansevieria trifasciata* and *Sansevieria cylindrica*. *Sansevieria trifasciata*, commonly known as "snake plant" or "in-law's tongue," is a species in the family Asparagaceae [2]. The leaves of STFs have zebra-like features, appearing straight, sword-shaped, and leathery, with cross-banded dark and light green shades, measuring 0.3–1 m in length [3]. STFs grow freely and are widely found in homes, parks, and woodlands. STFs are used as a source of strong white elastic fibers and are commonly used in the manufacture of rope, fishing line, cordage, fine webbing, bowstring, and clothing, where it can substitute for synthetic fibers. It was reported that STFs contain 56% cellulose, 34% hemicellulose, 6% lignin, and 4% moisture [4]. Due to their high cellulose content, STFs have good potential for use in the production of cellulose nanocrystals (CNCs).

Cellulose nanocrystals (CNCs) are a kind of nanomaterial derived from cellulose that have excellent characteristics, including good mechanical properties, nanometer sizes, high surface areas, renewability, non-toxicity, high thermal resistance, and good optical behavior [5–7]. Due to their excellent properties, CNCs have been extensively studied as promising candidates for potential applications in various fields, such as in drug delivery systems; as reinforcing agents for nanocomposites; as implants, conducting nanocomposites, or tissue engineering materials; in food packaging and coatings; and other uses [8].

The two most common groups of methods for producing CNCs are the mechanical and chemical techniques. The mechanical methods include high-pressure homogenization [9], high-intensity ultrasonication [10], micro-fluidization [11], and steam explosion [12], while

the chemical methods include acid hydrolysis [13], enzymatic hydrolysis [14], and oxidation [15]. Sulfuric acid hydrolysis is the most widely used method for producing CNCs from cellulose-fiber-based materials due to its ease of application and low energy consumption [16]. However, sulfuric acid hydrolysis has several disadvantages, such as not being eco-friendly, requiring a lot of water, involving the corrosion of equipment and excessive decomposition of cellulose, the lower thermal resistance of the resulting CNCs, the low yields, and the need for pre-treatment [17–20]. In addition to sulfuric acid hydrolysis, two oxidation methods have intensively been applied for the isolation of CNCs, namely the 2,2,6,6-tetramethylpiperidin-1-yloxy (TEMPO) and ammonium persulfate (APS) oxidation methods. The TEMPO method has several drawbacks, including the use of toxic reagents, the need for pre-treatment, and the limited oxidation position. The APS oxidation method has been applied to fabricate CNCs due to its simple one-step method and because it does not require pretreatment, has low toxicity and high solubility, and is cheaper [17]. CNCs have been successfully fabricated using the APS oxidation process from various cellulose-fiber-based materials, such as sugarcane bagasse pulp [21], cotton linters [22], an oil palm frond [23], Miscanthus x. Giganteus [24], lemon seeds [25], cotton pulp [26], and industrial denim waste [27]. The characteristics of the CNCs prepared with APS oxidation methods are strongly influenced by the oxidation parameters, such as the APS concentration, oxidation temperature, and oxidation time [19,23,27–30]. Hu et al. [28] investigated the influence of the oxidation temperature (65, 75, 85 °C) on the characteristics and drug delivery behaviors of CNCs prepared with the APS oxidation method from microcrystal celluloses (MCCs). They demonstrated that the highest crystallinity index (90.3%) and the maximum drug release rate of 94% within 420 h were achieved by the CNCs produced at 75 °C. The effect of the oxidation time (6, 8, 12, 16, 24 h) on the properties of CNCs prepared via APS oxidation from jute fibers was studied by Bashar et al. [19]. They reported that the crystallinity increased with increasing oxidation time up to 8 h and decreased with further oxidation time. Recently, Marwanto et al. [29] evaluated the influence of the oxidation time on the characteristics of CNCs isolated from Balsa and Kapok fibers via the APS oxidation method. They found that the higher crystallinity and thermal stability, along with the smaller size of the CNCs, resulted from increasing the oxidation time due to the removal of larger amorphous regions in the cellulose. In addition to the temperature and time, the APS concentration also affects the properties of CNCs. Zaini et al. [23] demonstrated that the crystallinity of CNCs increased with the increase in APS concentration, but their thermal stability decreased. Similar findings were also reported by Culsum et al. [27], who investigated the influences of the oxidation time and APS concentration on the characteristics of CNCs isolated from industrial denim waste. They demonstrated that the dimensions of CNCs decreased with an increase in oxidation time from 5 to 15 h, but their crystallinity increased. Moreover, the particle size and crystallinity decreased with increasing APS concentration, and the optimal oxidation process was achieved with 1.5 APS concentration at 60 °C for 15 h. Khanjanzadeh and Park [30] investigated the influences of oxidation parameters (APS concentration, temperature, and oxidation time) on the characteristics of CNCs produced from recycled medium-density fiberboard (r-MDF) fibers via the APS oxidation process. The optimal process for the obtained CNCs with the maximum yield and crystallinity was achieved at a 1.5 M APS concentration, an oxidation temperature of 70 °C, and an oxidation time of 16 h.

Although the APS method has been widely used for the preparation of CNCs from various natural fibers, to the best of our knowledge no studies on the fabrication of CNCs from STFs using APS oxidation have been previously published. In this work, the APS oxidation method was chosen to produce CNCs from STFs. This is because it is a simple, one-step procedure that requires no pretreatment, it uses a strong oxidizing agent that is cheap and has low long-term toxicity and high water solubility, and carboxylated cellulose nanocrystals can be formed directly [17]. The effects of the APS oxidation condition (APS concentrations and oxidation temperatures) on the characteristics of the resulting CNCs

were studied in this work. The properties of the resulting CNCs were investigated using SEM/EDS, TEM, FT-IR, XRD, and TGA.

2. Materials and Methods

2.1. Materials

Sansevieria trifasciata plants used in this study were supplied from the local farms around the city of Sleman, Yogyakarta, Indonesia. Ammonium persulfate ($(NH_4)_2S_2O_8$) and sodium hydroxide (99%) were purchased from Merck, New York, USA. As reported in our previous results [31], it was found that the STFs consisted of 43.53% cellulose, 29.27% hemicellulose, 5.20% lignin, 5.55% ash, and 16.45% moisture.

2.2. Extraction of Sansevieria trifasciata Fibers

The *Sansevieria trifasciata* fibers (STFs) were separated from the STF leaves by using a decorticator machine. The STFs leaves were fed into a fiber extraction machine known as a mechanical decorticator. The fibers were extracted and the pulps were separated. The decorticated fibers were then washed with water and dried in the sunlight to remove the moisture content. The dried STFs were cut 1 cm in length and then re-dried in an oven at 50 °C for 6 h. The dried STFs were ground and sieved within or below 50 mesh. Finally, the powder of STFs was obtained and further prepared to isolate CNCs. The schematic diagram of the extraction process of STFs is displayed in Figure 1.

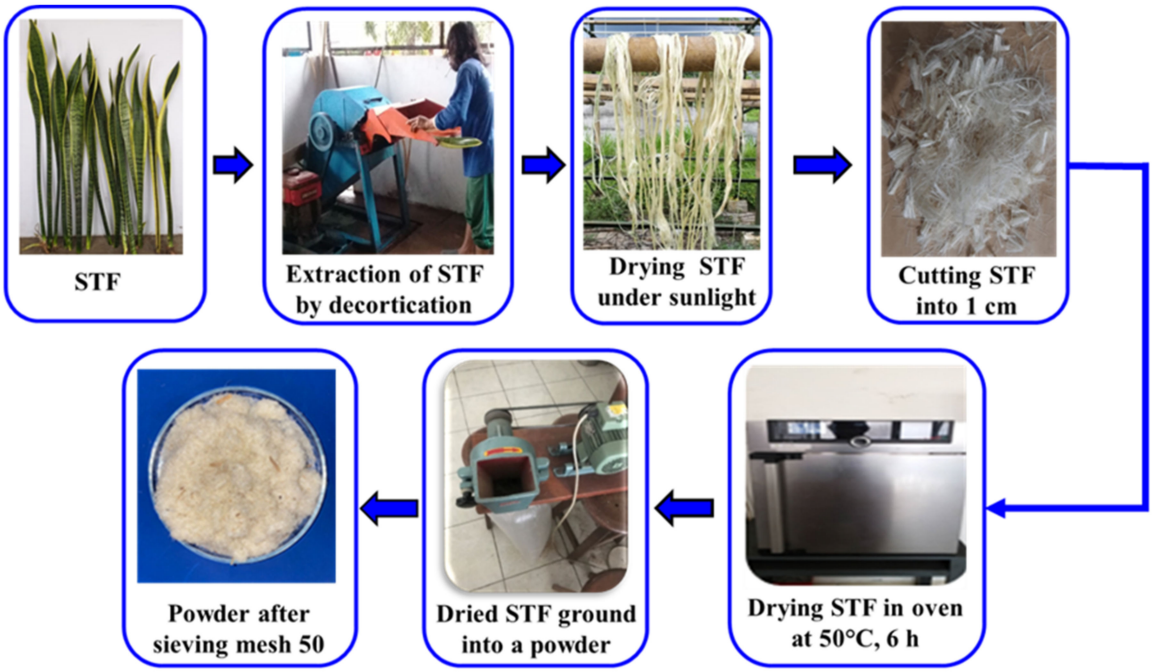

Figure 1. Extraction process of STFs.

2.3. Isolation of Cellulose Nanocrystals

CNCs were fabricated from the extracted STFs via the APS oxidation method following the previous method with a slight modification [22]. Briefly, 1 g of STF powder was put into 100 mL of APS solution at different concentrations (1.1, 1.5, and 1.9 M). The mixture was then heated at three different oxidation temperatures (60, 70, and 80 °C) and it was constantly mechanically stirred for a fixed period of 16 h. An aluminum foil was used to cover the reactor to avoid evaporation. The CNC suspension was rinsed using distilled water using a centrifuge at 4000 rpm for 10 min until the pH was 4. The suspension was homogenized using an ultrasonicator for 20 min with a power rate of 50%. The pH of the suspension was then adjusted to 8 by adding 1 M NaOH to prevent the aggregation of the crystals. Subsequently, the suspension was filtered using a Whatman glass microfiber filter

(grade 42, 2.5 µm). A part of the filtered CNC suspension was then characterized using TEM. The CNC suspension was freeze-dried at −18 °C overnight to collect the dried CNC powder. The dried CNC powder was then analyzed via FT-IR, XRD, and TGA. The APS oxidation process for preparing the CNCs is demonstrated in Figure 2.

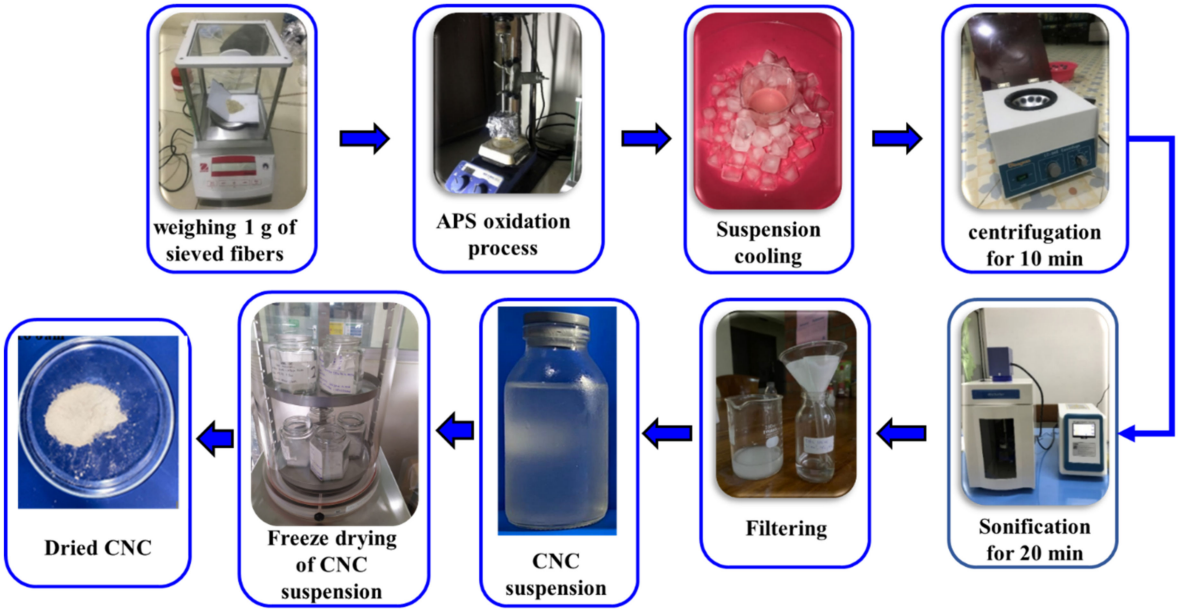

Figure 2. Isolation of CNCs from STFs via APS oxidation process.

2.4. Characterization

2.4.1. SEM/EDS Analysis

The surface morphology of the freeze-dried CNCs was examined using a scanning electron microscope (SEM) (JEOL type JSM-6510LA) operating at 10 kV. Before observation, the CNC powder was sputter-coated with platinum to obtain clearer SEM micrographs. The elemental composition of the selected CNCs (prepared at a 1.5 M APS concentration at 70 °C for 16 h) was analyzed using energy-dispersive X-ray spectroscopy (EDS).

2.4.2. Fourier Transform Infrared (FT-IR) Spectroscopy

The change of functional groups on the CNC surfaces was characterized using FT-IR. FT-IR spectra were collected using an infrared spectrophotometer (IRPrestige21 machine from Shimadzu) over a spectral range of 4000–400 cm^{-1}.

2.4.3. X-ray Diffraction (XRD) Analysis

The XRD patterns of STFs and CNCs were recorded using a MiniFlex 600 X-ray diffractometer (Rigaku, Tokyo, Japan) using Cu-Kα radiation (λ = 0.154 nm) operated at 40 kV and 30 mA. The XRD data were collected within a 2θ range of 10–50° at a scan rate of 0.3°/min. The crystallinity index was determined using the diffraction pattern and calculated following the Segal empirical method [32], as in Equation (1):

$$CrI = \frac{(I_{200} - I_{am})}{I_{200}} \times 100\% \quad (1)$$

where I_{200} is the maximum intensity of the (200) diffraction at a 2θ value range of about 22–23° and I_{am} is the minimum intensity of diffraction at a 2θ value range of around 18–19°.

2.4.4. Transmission Electron Microscopy (TEM)

The dimension and morphology of CNCs were observed using a JEM-1400 transmission electron microscope (JEOL Ltd., Tokyo, Japan) at a voltage of 120 kV. Here, 10 µL of

CNC solution was dropped onto a carbon-coated copper grid. ImageJ software was used to measure the diameter and length of the CNCs from the TEM images.

2.4.5. Thermogravimetric Analysis (TGA)

The thermal stability of CNCs was analyzed using TGA (TG/DTA Hitachi STA7300, Tokyo, Japan). The thermogravimetry (TG) and derivative thermogravimetry (DTG) curves were obtained from 30 to 600 °C at a constant heating rate of 10 °C/min under a nitrogen atmosphere.

3. Results and Discussion

3.1. Morphological Analysis by SEM/EDS

Figure 3 illustrates the SEM image of the CNCs produced at a 1.5 M APS concentration at 70 °C for 16 h. Most of the spherical and slightly rod-shaped structures of the CNCs can be observed in Figure 3. This structure was very different from the TEM images of CNCs, as discussed later, where rod-like particles with nanosized CNCs were observed. The large spherical structure of the CNCs observed from the SEM image was attributed to the CNCs' agglomeration. This agglomeration was related to the formation of inter-and intra-molecular hydrogen bonds between hydroxyl groups due to the hydrophilic nature of the CNCs [33]. Furthermore, Table 1 presents an elemental analysis of the CNCs taken from the SEM image (Figure 3).

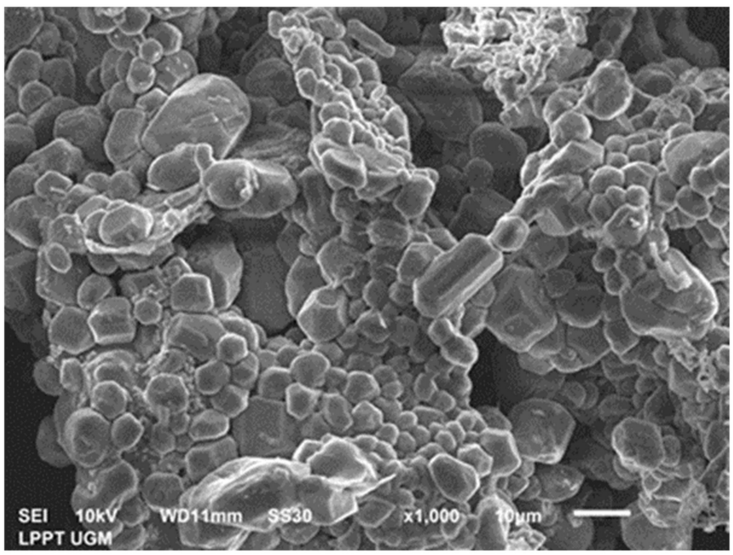

Figure 3. SEM image of CNCs prepared under a 1.5 M APS concentration at 70 °C for 16 h.

Table 1. Elements present in CNCs.

Element (wt%)				
C	N	O	Na	S
8.93	16.27	47.35	10.66	16.79

The peaks for carbon, nitrogen, oxygen, sodium, and sulfur corresponding to their binding energies are depicted in Figure 4. The existence of carbon and oxygen indicated these elements' presence in the CNCs. On the other hand, the appearances of nitrogen, sodium, and sulfur elements confirmed that the APS oxidation and the washing during centrifugation did not occur completely. This will influence the characteristics of the resulting CNCs, as discussed in the XRD analysis.

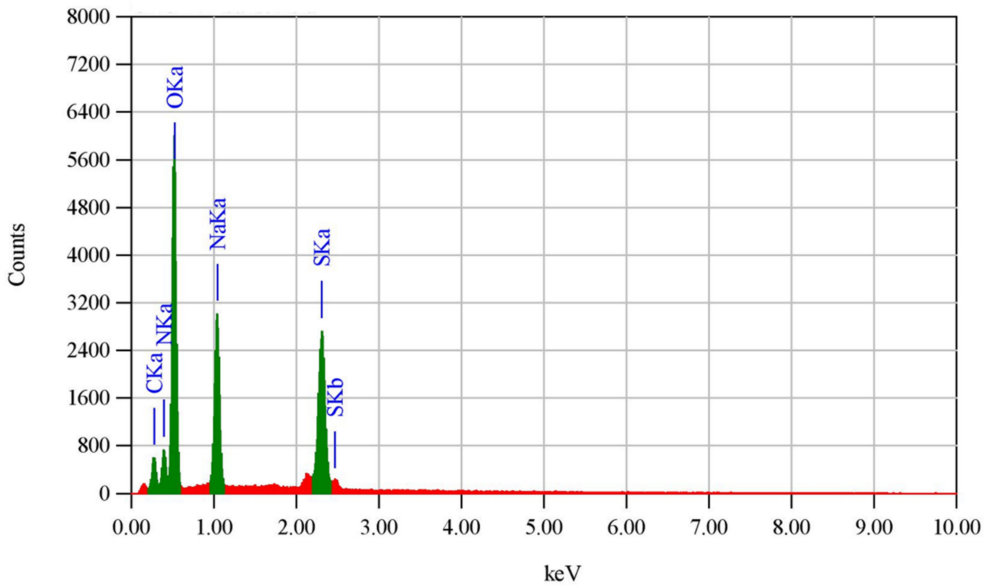

Figure 4. EDS diffraction for the elemental analysis of CNCs prepared under 1.5 M APS at 70 °C for 16 h.

3.2. Transmission Electron Microscopy

The dimension and morphology of the resulting CNCs produced from STFs were characterized using the TEM images. Figure 5 illustrates the TEM images of the obtained CNCs under different APS concentrations, i.e., 1.5 and 1.9 M, at a temperature of 70 °C for 16 h. Rod-like particles were exhibited by all CNCs, which indicated the successful isolation of individual CNCs from STF after the APS oxidation. The diameter and length distribution of the CNCs determined from TEM images are presented in Figure 6. The average diameter and length of the resulting CNCs under different APS concentrations ranged from 5 to 13 nm and from 96 to 211 nm, respectively. These findings were comparable to the results of previous studies [25,30]. The average diameter and length of the CNCs fabricated at the 1.5 M APS concentration, as shown in Figure 6a,b, were 7.43 ± 2.67 nm and 156.35 ± 54.58 nm, respectively. On the other hand, the average diameter and length of the CNCs produced at 1.9 M APS concentration, as presented in Figure 6c,d were 9.74 ± 2.75 and 139.47 ± 43.61 nm, respectively. This indicated that the average length decreased with increasing APS concentrations from 1.5 to 1.9 M at a constant oxidation temperature of 70 °C and oxidation time of 16 h. A similar finding was also reported by Khanjanzadeh and Park [30], where the average length of CNCs was decreased with an increase in the APS concentration from 1 to 2 M. The length reduction in CNCs obtained at the 1.9 M APS concentration was mainly attributed to the damage and removal of amorphous regions and or the crystalline regions of the cellulose during the APS oxidation [30]. The cleavage of the amorphous domain through the hydrolysis of the 1,4-β bonds of the cellulose chain and oxidation of the C6 hydroxyl group to form a carboxyl group occurs by the formation of sulfate radical anions (SO_4^-), hydrogen peroxide (H_2O_2), and hydrogen sulfate ions (HSO_4^-) [34]. According to Filipova et al. [35] and Oun and Rhim [36], the dimensions and morphology of the CNCs are mainly affected by the cellulose resources, isolation method, and process parameters. In APS oxidation, it has been well documented that the dimensions and morphology of CNCs are strongly affected by factors such as the APS concentration, oxidation temperature, and oxidation time [28].

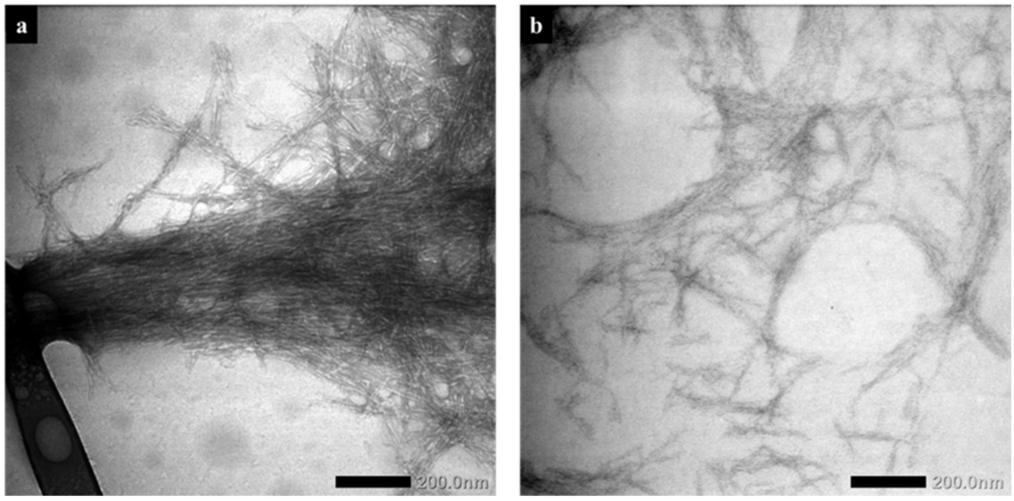

Figure 5. TEM images of CNCs produced at different APS concentrations: (**a**) 1.5 M; (**b**) 1.9 M.

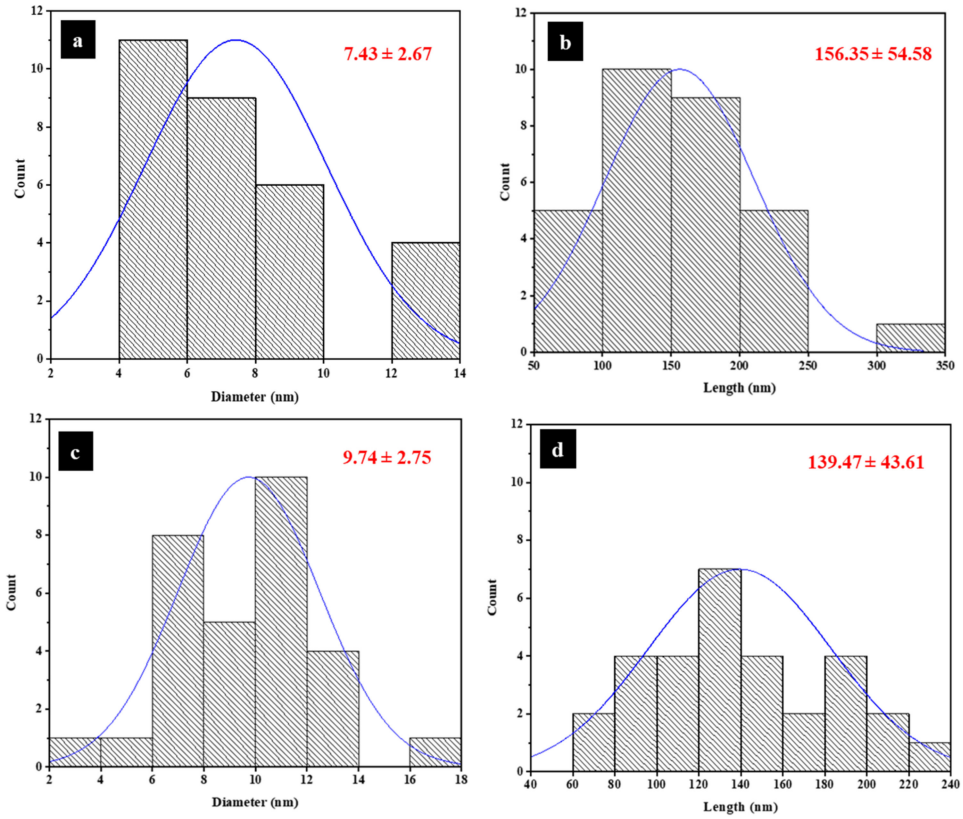

Figure 6. Diameter and length distribution of CNCs under different APS concentrations at 70 °C for 16 h: (**a**,**b**) 1.5 M; (**c**,**d**) 1.9 M.

3.3. Fourier Transform Infrared (FT-IR) Spectroscopy

Figure 7 demonstrates the FT-IR spectra of STFs and CNCs produced under different APS concentrations and oxidation temperatures.

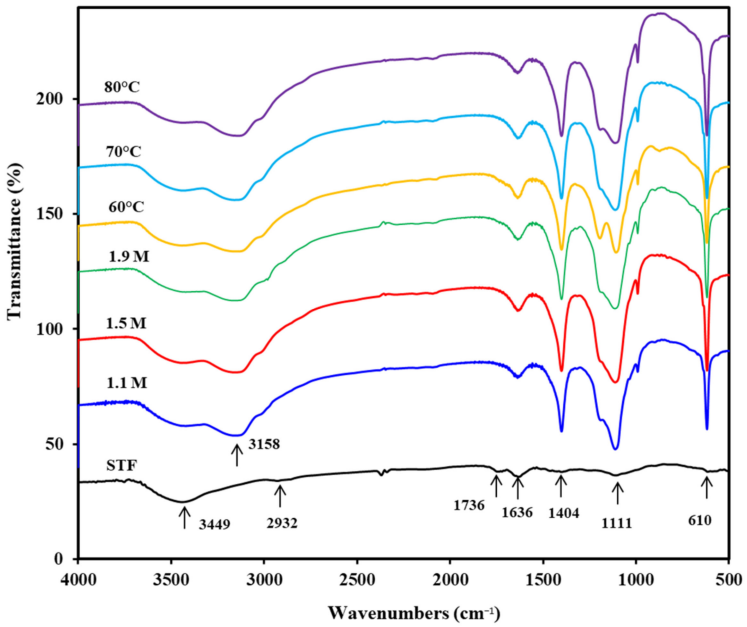

Figure 7. FTIR spectra of STFs and CNCs obtained under different APS concentrations at 70 °C for 16 h and under different oxidation temperatures with a 1.5 M APS concentration for 16 h.

The FT-IR spectrum of STFs exhibited peaks at 3448, 2932, 1736, 1636, 1404, 1111, and 610 cm^{-1}. The peak at 3448 cm^{-1} was related to the OH stretching vibration in the cellulose [21,36,37], while the peak at 2932 cm^{-1} was assigned to CH_2 symmetric and asymmetric stretching vibrations, respectively [36–39]. The peak at 1736 cm^{-1} was related to the C=O stretching vibration of the acetyl ester and uronic groups of hemicellulose, as well as the ester linkage of the carboxylic groups of the ferulic and p-coumaric groups in the lignin [38,40,41]. The peak observed at 1636 cm^{-1} was related to the adsorbed water due to the abundant presence of hydrophilic hydroxide radicals in the cellulose [42,43]. The peaks at 1404 and 1111 cm^{-1} were ascribed to the asymmetric bending of CH_3 [44] and glucose ring skeletal vibrations [26], respectively. The peak at 610 cm^{-1} was assigned to the aromatic -CH stretching vibration [45].

As presented in Figure 7, it can be observed that all CNCs revealed a similar characteristic band with the STFs. This suggested no destruction of the main cellulose structures during the APS oxidation process [25,36,39]. Furthermore, the peak at 1736 cm^{-1} observed in the STF spectra disappeared in all CNC spectra, confirming the effective removal of amorphous components from the STFs during the APS oxidation process [38,39,46]. In addition, all the CNCs exhibited a small peak at 1189 cm^{-1}, indicating the asymmetric C–O–C bridge stretching [30]. From Figure 7, it can also be observed that the peaks at 1404, 1189, 1111, and 610 cm^{-1} appeared in all the CNCs and exhibited more intensity compared to those of the STFs. This indicated the removal of non-cellulosic components (hemicellulose and lignin) during the oxidation and an improvement in the content of the crystalline cellulose [30]. Furthermore, similar spectra were demonstrated by all CNCs at various APS concentrations, indicating no effect of different concentrations of APS in this work. Compared to the CNCs produced at 60 °C, the CNCs prepared at 80 °C showed a lower intensity at a peak of 1189 cm^{-1}, indicating the lower cellulose crystalline content. This was because at higher oxidation temperatures, not only the amorphous regions but also parts of the crystalline regions were removed during APS oxidation. This promoted the hydrolytic cleavage of the glycosidic bond and then led to the reduced crystallinity index [47]. This was confirmed by the XRD results discussed later. Overall, the FT-IR results indicated that the APS oxidation did not change the cellulose structure but the oxidation temperature affected the removal of the amorphous components in the cellulose.

3.4. X-ray Diffraction (XRD)

Figure 8 depicts the XRD pattern of STFs. The STFs exhibited diffraction peaks at 2θ = 16, 22.2, and 34.4° corresponding to (110), (200), and (400) planes of the typical structure of cellulose Iβ, respectively [8,48].

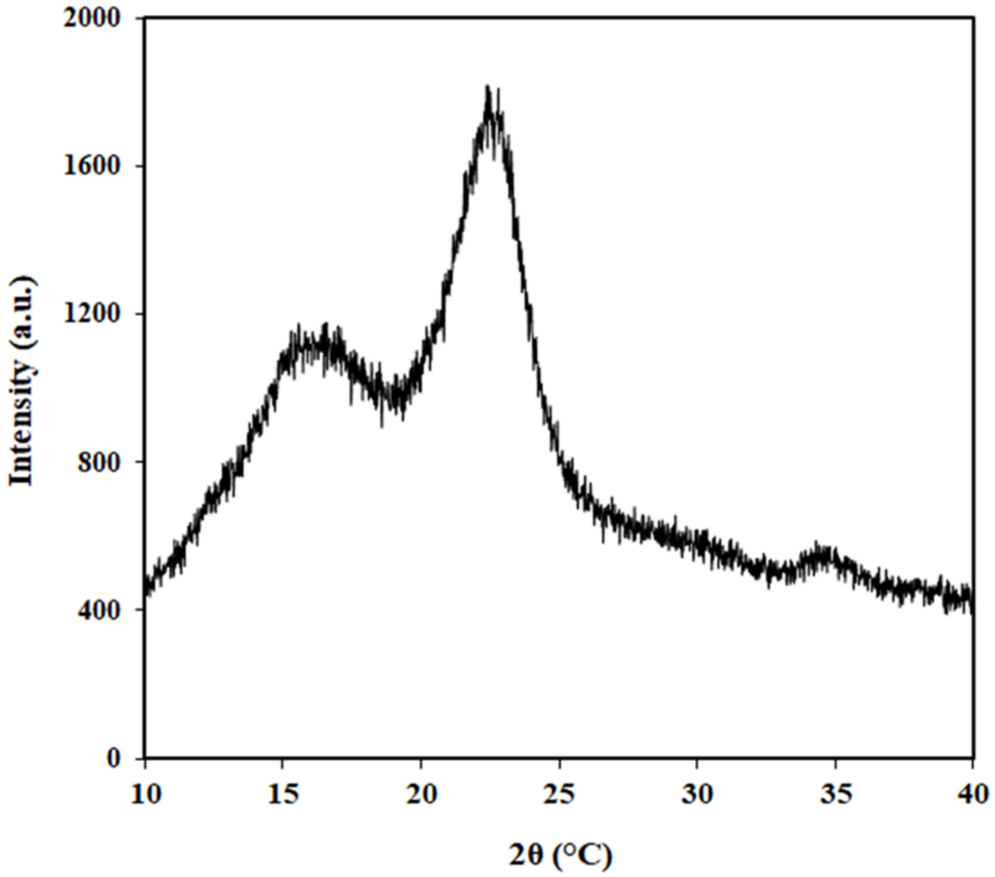

Figure 8. XRD patterns of STFs.

Furthermore, the XRD profiles of all CNCs produced under different APS concentrations and oxidation temperatures are displayed in Figure 9a,b, respectively. All CNCs showed a similar diffraction pattern, where a larger number of peaks were observed. This indicated an increase in cellulose crystalline contents in all CNCs. The presence of the peaks confirmed the crystalline structure of cellulose I, as presented by peaks at 2θ = 16, 22.2, and 34.4° still being maintained in all CNCs after APS oxidation. Moreover, some diffraction peaks at 2θ = 19.8 and 37° were also shown by all CNCs, which corresponded to the $(10\bar{1})$ and (004) lattice planes of cellulose II, respectively [49]. This revealed that some of the cellulose I was converted to cellulose II during APS oxidation. The existence of sodium salt that was not completely removed during washing, as confirmed by the EDS analysis, might be believed to be responsible for the partial conversion from cellulose I to II (Figure 3). Cellulose I can change to cellulose II during alkali treatment, in which the chains of cellulose II have an antiparallel arrangement, producing a more stable structure [50].

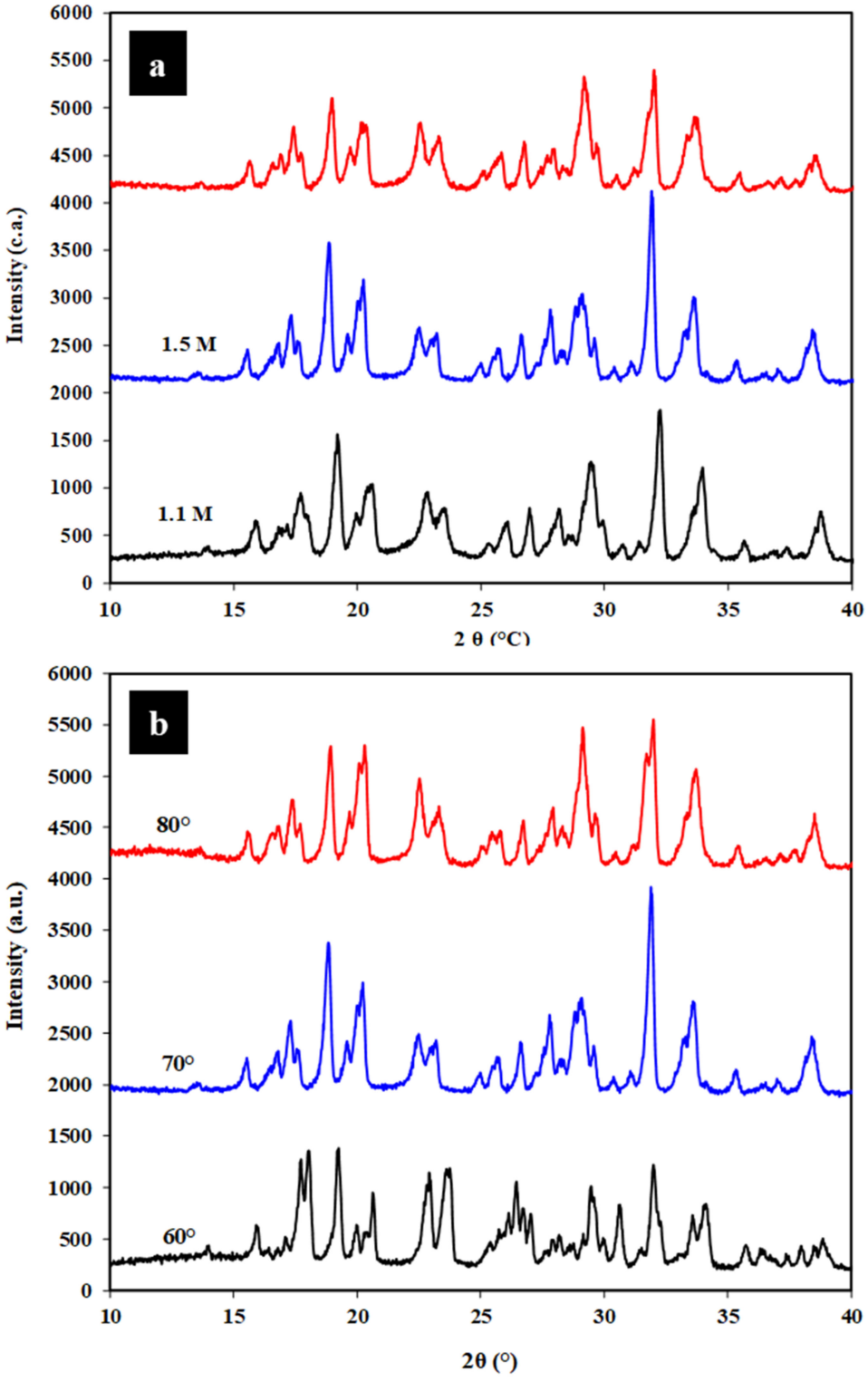

Figure 9. XRD patterns of CNCs obtained under different (**a**) APS concentrations at 70 °C for 16 h and (**b**) oxidation temperatures with a 1.5 M APS concentration for 16 h.

Table 2 summarizes the crystallinity index values of STFs and all CNCs fabricated at various APS concentrations and oxidation temperatures.

Table 2. Crystallinity index of STFs and CNCs prepared under different APS concentrations at 70 °C for 16 h and under different oxidation temperatures with 1.5 APS concentration for 16 h.

Sample	Crystallinity Index (%)
STFs	52.4
CNC 1.1 M	80.0
CNC 1.5 M	87.4
CNC 1.9 M	83.4
CNC 60 °C	76.2
CNC 70 °C	87.4
CNC 80 °C	61.4

The crystallinity index was calculated by using the Segal equation (Equation (1)). As demonstrated in Table 2, the crystallinity index of the STFs was 52.4%, while the crystallinity index values of CNCs prepared under different APS concentrations of 1.1, 1.5, and 1.9 M were 80, 87.4, and 83.4%, respectively. This indicated that the crystallinity index values of all CNCs were much higher than that of the STFs. This was related to the successful removal of non-crystalline components (hemicellulose and lignin) in the STFs during the APS oxidation process [36]. This suggested that APS oxidation improved the crystallinity index of the STFs. During oxidation, the sulfate radical anions ($SO4^{2-}$), hydrogen peroxide (H_2O_2), and hydrogen sulfate ions (HSO_4^-) attacked and penetrated the more accessible amorphous regions, causing the hydrolytic cleavage of glycosidic bonds, and ultimately producing individual crystallites [18]. From Table 2, it can be seen that the CNCs produced at a 1.5 M APS concentration exhibited the highest crystallinity index values among all CNCs. This was probably related to the most effective removal of residual amorphous components in the cellulose during the APS oxidation [30]. Furthermore, the crystallinity index of CNCs was increased from 76.2% to 87.4% when the oxidation temperature was increased from 60 to 70 °C. However, the crystallinity index of CNCs decreased to 61.4% as the oxidation temperature increased up to 80 °C. The reduced crystallinity index at 80 °C was associated with the partial removal of the crystalline structure of the cellulose [18,37,51,52]. Overall, it could be concluded that the crystallinity index of the CNCs was strongly influenced by both the APS concentrations and oxidation temperatures. These findings were in good agreement with the previous studies [30]. Using a similar method of APS oxidation, the crystallinity index of the resulting CNCs was higher (87.4%) compared to that of other CNCs extracted from other cellulose sources such as oil palm frond (52.4%) [23], balsa (57.6%) and kapok (60.7%) [29], recycled medium-density fiberboard (63%) [30], sugarcane bagasse (76.5%) [21], borer powder of bamboo (69.8%) [39], Miscanthus x. Giganteus (70%) [24], lemon seeds (74.4%) [25], and industrial denim waste (83%) [27]. However, it was lower than the value for cotton liner (93.5%) [36]. The differences in crystallinity index were attributed to the different cellulose sources. From Table 2, it can also be seen that the optimal oxidation process with the highest crystallinity index (87.4%) was achieved with the 1.5 M APS concentration at 70 °C and with an oxidation time of 16 h. According to Montane et al. [53] and Thambiraj and Shankaran [54], both the strength and stiffness of the CNC-reinforced nanocomposites were increased by increasing the crystallinity index of the CNCs. In addition, the tensile strength was enhanced with an increase in the higher crystallinity index of the cellulose nanofibers [55]. Therefore, with this high crystallinity (87.4%), the CNCs have great potential for applications as nanocomposite reinforcements. Therefore, compared to the two-step oxidation method as reported by Yang et al. [24], where the bleaching and oxidation processes were performed, producing CNCs with lower crystallinity (70%), the one-step oxidation approach in this work resulted in CNCs with higher crystallinity (87.4%) and simplicity, without the chemical pretreatment. These were the advantages of the method used in this work compared to the two-step oxidation method involving the bleaching treatment and ammonium persulfate oxidation [24]. The CNCs prepared under the optimal oxidation parameters in this work showed higher crystallinity (87.4%) compared to the CNCs produced via TEMPO-mediated oxidation

from the bleached sugarcane bagasse pulp (40%) and lemon seeds (66.14%), as reported by previous researchers [21,25]. This was associated with greater decomposition of the amorphous regions of the cellulose during the APS oxidation process.

3.5. Thermogravimetry Analysis

Figure 10a,b illustrate the TGA and DTG thermograms of STFs and CNCs fabricated via APS oxidation at various APS concentrations, respectively.

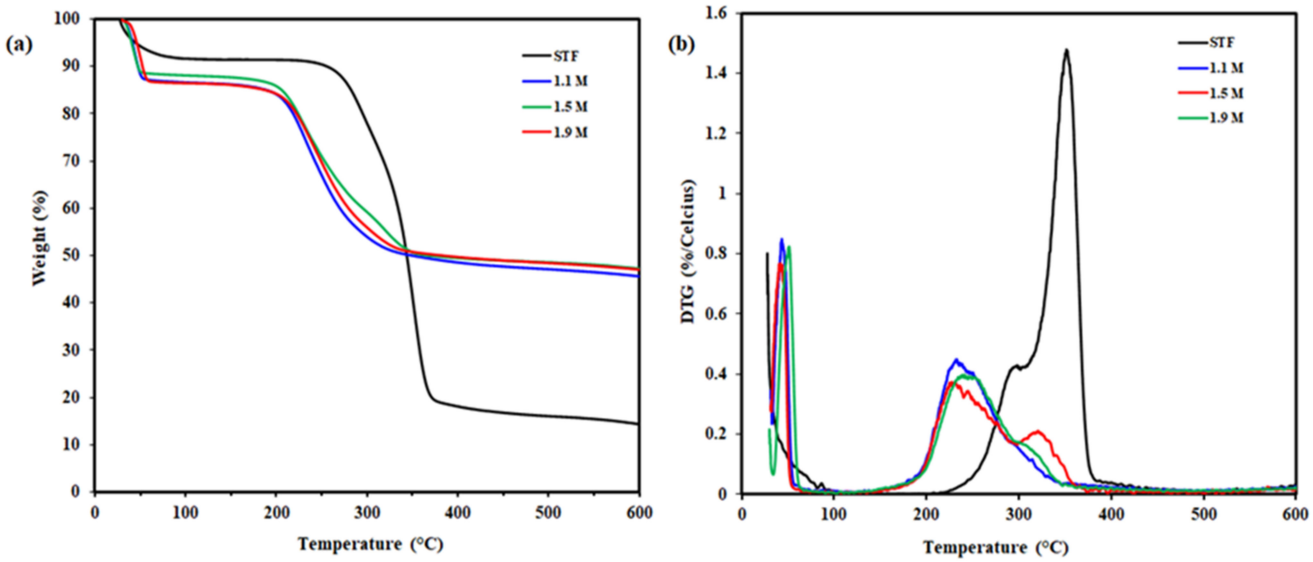

Figure 10. TGA (**a**) and DTG (**b**) thermograms of STFs and CNCs under different APS concentrations at 70 °C for 16 h.

The TGA and DTG thermograms of CNCs produced at different oxidation temperatures are depicted in Figure 11a,b, respectively. The onset degradation temperature (T_{onset}), the maximum degradation temperature (T_{max}), and the residual mass values ($W_{residue}$) as the thermal parameters are listed in Table 3. As can be seen in Figures 10a and 11a, all samples exhibited a similar appearance and degradation patterns. The initial weight loss (7–20%) was exhibited by all samples at the temperature range of 30–100 °C. This was associated with the vaporization of the absorbed water [30]. Furthermore, the main weight loss in the temperature range of 200–400 °C was assigned to the main decomposition of the cellulose [30]. This was associated with the breakdown of the cellulose chain through both depolymerization and dehydration reactions, as well as the decomposition of glycosyl units in the cellulose chain [56]. Furthermore, the decomposition that occurred above 400 °C was associated with both the oxidation and short-chain cleavage of residues, changing them to lower molecular weight volatile products [57,58].

Table 3. Thermal properties of STFs and CNCs prepared under different APS concentrations at 70 °C for 16 h and under different oxidation temperatures with a 1.5 M APS concentration for 16 h.

Sample	T_{onset} (°C)	T_{max1} (°C)	T_{max2} (°C)	$W_{residue}$ (%)
STF	270	295	352	14.3
CNC 1.1 M	203	233	-	45.6
CNC 1.5 M	206	229	320	47.3
CNC 1.9 M	209	244	318	46.9
CNC 60 °C	220	260	402	32.8
CNC 70 °C	206	229	320	47.3
CNC 80 °C	207	232	329	48.2

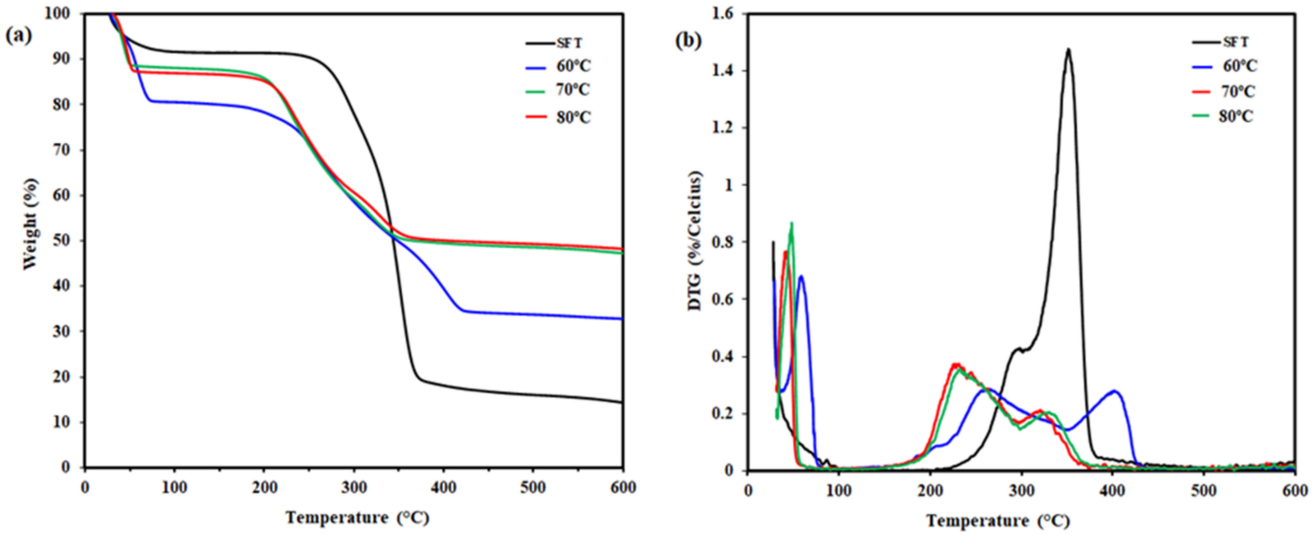

Figure 11. TGA (**a**) and DTG (**b**) thermograms of STFs and CNCs under different oxidation temperatures with a 1.5 M APS concentration for 16 h.

From the DTG thermogram of the STF (Figures 10b and 11b), it can be observed that there was a small broad peak known as T_{max1} that was attributed to the degradation of non-cellulosic constituents such as hemicellulose and lignin [59]. The hemicelluloses degraded quickly in the temperature range of 220–315 °C, whereas the cellulose decomposed in the range of 315–400 °C and lignin degraded over the entire temperature range [60]. The lower degradation temperature of the hemicelluloses was ascribed to the acetyl groups (-C_2H_3O) present in their structure [30]. Table 3 summarizes the thermal parameters such as T_{onset}, T_{max1}, T_{max2}, and $W_{residue}$ of the STFs and CNCs produced via APS oxidation at different concentrations and oxidation temperatures. It was found that the T_{onset} value of the STFs was 270 °C, while the T_{onset} values of CNCs fabricated at different concentrations of 1.1, 1.5, and 1.9 M were 203, 206, and 209 °C, respectively. This showed that the T_{onset} values of the CNCs were much lower than that of the STFs, suggesting lower thermal stability for the CNCs. Similar findings were also obtained in other reports [25,30,36]. The lower thermal stability of the CNCs might be related to the improvement in the heat transfer rate due to the increase in surface area as a result of the smaller particle size of the CNCs [61]. In addition, the CNCs exhibited a lower thermal degradation range (200–250 °C), which might be due to the incorporation of sodium carboxyl groups on the CNC surfaces during the oxidation process leading to a reduction in the thermal degradation temperature [22,62]. A similar thermal degradation behavior was also shown by the CNCs prepared using the TEMPO-mediated oxidation method, with which the thermal stability of the CNCs was lower than their native cellulose [62–64]. Compared to the CNCs produced using the TEMPO-mediated oxidation method as reported by Zhang et al. [21], the resulting CNCs in this study exhibited higher thermal stability. This might be related to the higher crystallinity of the resulting CNCs in this work. According to Cheng et al. [37] and Poletto et al. [65], the thermal stability of the CNCs was strongly influenced by the surface structure, size, crystallinity, drying, and isolation methods. Except for the CNCs produced at 1.1 M APS concentration, two major degradation peaks, namely T_{max1} and T_{max2}, were observed in the STFs and all CNCs, as shown in Figures 10b and 11b. The major degradation peak presented by the STFs, referred to as the T_{max2} of 352 °C, was attributed to the main decomposition of the cellulose [30]. All CNCs demonstrated thermal degradation over a lower temperature range (T_{max1}) of 229–295 °C relating to the incorporation of -COO-Na^+ groups to the CNC surfaces [36,56]. Furthermore, the thermal decomposition over the higher temperature range of 318–352 °C, known as T_{max2}, was associated with the degradation of the backbone structure of the cellulose (-OH groups) [36,50]. As presented in Table 3, the T_{onset} value of the CNCs was increased slightly by increasing the APS

concentration but was decreased as the oxidation temperature increased. On the other hand, the T_{max1} and T_{max2} values of the CNCs were decreased with the increased APS concentration and oxidation temperatures. The thermal degradation of the CNCs was attributed to the different amounts of sodium carboxylate groups on the CNC surfaces and the different dimensions of the CNCs [30]. Therefore, the thermal resistance of the CNCs prepared via APS oxidation was influenced strongly by the oxidation conditions. The existence of sodium carboxylate groups at the C6 primary hydroxyls on the CNC surfaces reduced their thermal stability. The nanometer dimensions, reduced molecular weight, high specific surface area, and increased heat transfer rate were believed to be responsible for the lower thermal stability of the CNCs [66–68]. The thermal stability of the resulting CNCs was comparable with the previous studies [30] but was higher compared with the CNCs fabricated by acid hydrolysis [37,39].

From Table 3, all the CNCs had much higher final residues at 600 °C ($W_{residue}$) compared to the STF. This was related to the high crystallinity of all CNCs, an increase in carbon content, the presence of NaOH that was included in the CNC isolation process, and the incorporation of the sodium carboxylate groups on the CNC surfaces, which acted as a flame retardant [36,37,39,67,69]. The existence of the Na element was confirmed from the EDS results in Table 1. This finding was in good accordance with the previous studies [36,39], where all CNCs had a much higher final residue at 600 °C than the native cellulosic materials. As demonstrated in Table 3, the final residue of the CNCs was increased when the APS concentration was increased up to 1.5 M and then decreased at 1.9 M. This was ascribed to the highest crystallinity index of the CNCs produced at a concentration of 1.5 M APS, as confirmed from XRD results in Table 2. Furthermore, as shown in Table 3, the final residues of CNCs prepared at different oxidation temperatures of 60, 70, and 80 °C were 32.8, 47.3, and 48.2%, respectively. This indicated that the final residue of the CNCs was increased with the increasing oxidation temperatures. This was due to the higher crystallinity index when the oxidation temperature was increased, as shown by the XRD results.

4. Conclusions

In this work, CNCs were directly fabricated from STFs via APS oxidation without any pretreatment. The influences of the oxidation parameters (APS concentrations and oxidation temperature) on the characteristics of the CNCs were evaluated. The TEM images exhibited the formation of rod-like CNCs. All CNCs showed higher crystallinity index values (61–87%) compared to the STFs (52%). The crystallinity index of CNC was increased when the APS concentration increased from 1.1 to 1.5 M, while it was decreased at the APS concentration of 1.9 M. A similar effect was shown for the oxidation temperature. Therefore, it was proven that the CNCs' characteristics were affected significantly by both the APS concentration and oxidation temperature. The highest crystallinity was obtained at the oxidation temperature of 70 °C, oxidation time of 16 h, and a 1.5 M APS concentration. Based on the thermal analysis, all CNCs exhibited lower thermal stability compared with the STFs due to the nano dimensions of the CNCs, their reduced molecular weight, their high specific surface area, and their high rate of heat transfer. The CNCs obtained from this work, which had high crystallinity (87.4%), showed great potential as nanocomposite-reinforcing agents.

Author Contributions: Conceptualization, K.; methodology, N.L.I.; validation, K.; investigation, N.L.I.; resources, K.; writing—original draft preparation, N.L.I.; writing—review and editing, K. All authors have read and agreed to the published version of the manuscript.

Funding: This work was supported by the Minister of Education, Culture, Research, and Technology, Republic of Indonesia, and Universitas Gadjah Mada, Yogyakarta, under the research grant of Hibah Penelitian Dasar Unggulan Perguruan Tinggi (PDUPT) (contract no. 1715/UN1/DITLIT/DITLIT/PT/2021).

Institutional Review Board Statement: Not applicable.

Informed Consent Statement: Not applicable.

Data Availability Statement: The data presented in this study are available on request from the corresponding author.

Acknowledgments: The authors would like to acknowledge the Department of Mechanical and Industrial Engineering, Universitas Gadjah Mada, Yogyakarta, Indonesia.

Conflicts of Interest: The authors declare no conflict of interest.

References

1. Kanimozhi, M. Investigating the physical characteristics of sansevieria trifasciata fibre. *Int. J. Sci. Res. Publ.* **2011**, *1*, 1–4.
2. Rwawiire, S.; Tomkova, B. Morphological, thermal, and mechanical characterization of Sansevieria trifasciata fibers. *J. Nat. Fibers* **2015**, *12*, 201–210. [CrossRef]
3. Keng, H.; Chin, S.C.; Tan, H.T.W. *The Concise Flora of Singapore: Monocotyledons*; Singapore University Press: Singapore, 1998; Volume II.
4. Mardiyati; Steven; Rizkiansyah, R.R.; Senoaji, A.; Suratman, R. Effects of alkali treatment on the mechanical and thermal properties of Sansevieria trifasciata fiber. *AIP Conf. Proc.* **2016**, *1725*, 020043.
5. Habibi, Y.; Lucia, L.A.; Rojas, O.J. Cellulose nanocrystals: Chemistry, self-assembly, and applications. *Chem Rev.* **2010**, *110*, 3479–3500. [CrossRef] [PubMed]
6. Moon, R.J.; Martini, A.; Nairn, J.; Simonsen, J.; Youngblood, J. Cellulose nanomaterials review: Structure, properties, and nanocomposites. *Chem. Soc. Rev.* **2011**, *40*, 3941–3994. [CrossRef]
7. Csiszar, E.; Kalic, P.; Kobol, A.; Eduardo de Paulo, F. The effect of low frequency ultrasound on the production and properties of nanocrystalline cellulose suspensions and films. *Ultrason. Sonochemistry* **2016**, *31*, 473–480. [CrossRef]
8. Khanjanzadeh, H.; Behrooz, R.; Bahramifar, N.; Gindl-Altmutter, W.; Bacher, M.; Edler, M.; Griessere, T. Surface chemical functionalization of cellulose nanocrystals by 3-aminopropyltriethoxysilane. *Int. J. Biol. Macromol.* **2018**, *106*, 1288–1296. [CrossRef]
9. Jonoobi, M.; Oladi, R.; Davoudpour, Y.; Oksman, K.; Dufresne, A.; Hamzeh, Y.; Davoodi, R. Different preparation methods and properties of nanostructured cellulose from various natural resources and residues: A review. *Cellulose* **2015**, *22*, 935–969. [CrossRef]
10. Li, W.; Yue, J.Q.; Liu, S.X. Preparation of nanocrystalline cellulose via ultrasound and its reinforcement capability for poly(vinyl alcohol) composites. *Ultrason. Sonochem.* **2012**, *19*, 479–485. [CrossRef]
11. Khan, A.; Vu, K.D.; Chauve, G.; Bouchard, J.; Riedl, B.; Lacroix, M. Optimization of microfluidization for the homogeneous distribution of cellulose nanocrystals (CNCs) in biopolymeric matrix. *Cellulose* **2014**, *21*, 3457–3468. [CrossRef]
12. Cherian, B.M.; Leão, A.L.; de Souza, S.F.; Thomas, S.; Pothan, L.A.; Kottaisamy, M. Isolation of nanocellulose from pineapple leaf fibres by steam explosion. *Carbohydr. Polym.* **2010**, *81*, 720–725. [CrossRef]
13. Kusmono; Listyanda, R.F.; Wildan, M.W.; Ilman, M.N. Preparation and characterization of cellulose nanocrystal extracted from ramie fibers by sulfuric acid hydrolysis. *Heliyon* **2020**, *6*, e05486. [CrossRef]
14. Ribeiro, R.S.A.; Pohlmann, B.C.; Calado, V.; Bojorge, N.; Pereira, N., Jr. Production of nanocellulose by enzymatic hydrolysis: Trends and challenges. *Eng. Life Sci.* **2019**, *19*, 279–291. [CrossRef] [PubMed]
15. Sun, X.; Wu, Q.; Ren, S.; Lei, T. Comparison of highly transparent all-cellulose nanopaper prepared using sulfuric acid and TEMPO-mediated oxidation methods. *Cellulose* **2015**, *22*, 1123–1133. [CrossRef]
16. Espino, E.; Cakir, M.; Domenek, S.; Roma´n-Gutie´rrez, A.D.; Belgacem, N.; Bras, J. Isolation and characterization of cellulose nanocrystals from industrial by-products of Agave tequilana and barley. *Ind. Crops Prod.* **2014**, *62*, 552–559. [CrossRef]
17. Leung, A.C.W.; Hrapovic, S.; Lam, E.; Liu, Y.; Male, K.B.; Mahmoud, K.A.; Luong, J.H.T. Characteristics and properties of carboxylated cellulose nanocrystals prepared from a novel one-step procedure. *Small* **2011**, *7*, 302–305. [CrossRef] [PubMed]
18. Du, H.; Liu, C.; Mu, X.; Gong, W.; Lv, D.; Hong, Y.; Si, C.; Li, B. Preparation and characterization of thermally stable cellulose nanocrystals via a sustainable approach of FeCl3-catalyzed formic acid hydrolysis. *Cellulose* **2016**, *23*, 2389–2407. [CrossRef]
19. Bashar, M.M.; Zhu, H.; Yamamoto, S.; Mitsuishi, M. Highly carboxylated and crystalline cellulose nanocrystals from jute fiber by facile ammonium persulfate oxidation. *Cellulose* **2019**, *26*, 3671–3684. [CrossRef]
20. Ji, H.; Xiang, Z.; Qi, H.; Han, T.; Pranovich, A.; Song, T. Strategy towards one-step preparation of carboxylic cellulose nanocrystals and nanofibrils with high yield, carboxylation and highly stable dispersibility using innocuous citric acid. *Green Chem.* **2019**, *21*, 1956–1964. [CrossRef]
21. Zhang, K.; Sun, P.; Liu, H.; Shang, S.; Song, J.; Wang, W. Extraction and comparison of carboxylated cellulose nanocrystals from bleached sugarcane bagasse pulp using two different oxidation methods. *Carbohydr. Polym.* **2016**, *138*, 237–243. [CrossRef]
22. Mascheroni, E.; Rampazzo, R.; Ortenzi, M.A.; Piva, G.; Bonetti, S.; Piergiovanni, L. Comparison of cellulose nanocrystals obtained by sulfuric acid hydrolysis and ammonium persulfate, to be used as coating on flexible food-packaging materials. *Cellulose* **2016**, *23*, 779–793. [CrossRef]
23. Zaini, L.H.; Febrianto, F.; Wisata, N.J.; Maulana, M.M.I.; Lee, S.H.; Kim, N.H. Effect of ammonium persulfate concentration on characteristics of cellulose nanocrystals from oil palm frond. *J. Korean Wood Sci. Technol.* **2019**, *47*, 597–606. [CrossRef]
24. Yang, H.; Zhang, Y.; Kato, R.; Rowan, S.J. Preparation of cellulose nanofibers from Miscanthus x. Giganteus by ammonium persulfate oxidation. *Carbohydr. Polym.* **2019**, *212*, 30–39. [CrossRef] [PubMed]

25. Zhang, H.; Chen, Y.; Wang, S.; Ma, L.; Yu, Y.; Dai, H.; Zhang, Y. Extraction and comparison of cellulose nanocrystals from lemon (*Citrus limon*) seeds using sulfuric acid hydrolysis and oxidation methods. *Carbohydr. Polym.* **2020**, *238*, 116180. [CrossRef] [PubMed]
26. Liu, Y.; Liu, L.; Wang, K.; Zhang, H.; Yuan, Y.; Wei, H.X.; Wang, X.; Duan, Y.; Zhuo, L.; Zhang, J. Modified ammonium persulfate oxidations for efficient preparation of carboxylated cellulose nanocrystals. *Carbohydr. Polym.* **2020**, *229*, 115572. [CrossRef]
27. Culsum, N.T.U.; Melinda, C.; Leman, I.; Wibowo, A.; Budhi, Y.W. Isolation and characterization of cellulose nanocrystals (CNCs) from industrial denim waste using ammonium persulfate. *Mater. Today Commun.* **2021**, *26*, 101817. [CrossRef]
28. Hu, S.; Qin, Z.; Cheng, M.; Chen, Y.; Liu, J.; Zhang, Y. Improved properties and drug delivery behaviors of electrospun cellulose acetate nanofibrous membranes by introducing carboxylated cellulose nanocrystals. *Cellulose* **2018**, *25*, 1883–1898. [CrossRef]
29. Marwanto, M.; Maulana, M.I.; Febrianto, F.; Wistara, N.J.; Nikmatin, S.; Masruchin, N.; Zaini, L.H.; Lee, S.H.; Kim, N.H. Effect of oxidation time on the properties of cellulose nanocrystals prepared from Balsa and Kapok fibers using ammonium persulfate. *Polymers* **2021**, *13*, 1894. [CrossRef]
30. Khanjanzadeh, H.; Park, B.-D. Optimum oxidation for direct and efficient extraction of carboxylated cellulose nanocrystals from recycled MDF fibers by ammonium persulfate. *Carbohydr. Polym.* **2021**, *251*, 117029. [CrossRef]
31. Indirasetyo, N.L. Production and Characterization of Cellulose Nanocrystal from Sansevieria Fibers via Ammonium Persulfate Oxidation method. Bachelor's Thesis, Universitas Gadjah Mada, Yogyakarta, Indonesia, 2021.
32. Segal, L.; Creely, J.J.; Martin, A.E.; Conrad, C.M. An empirical method for estimating the degree of crystallinity of native cellulose using the X-ray Diffractometer. *Textil. Res. J.* **1959**, *29*, 786–794. [CrossRef]
33. Mondal, S. Preparation, properties and applications of nanocellulosic materials. *Carbohydr. Polym.* **2017**, *163*, 301–316. [CrossRef] [PubMed]
34. Khanjanzadeh, H.; Park, B.-D. Characterization of carboxylated cellulose nanocrystals from recycled fiberboard fibers using ammonium persulfate oxidation. *J. Korean Wood Sci. Technol.* **2020**, *48*, 231–244. [CrossRef]
35. Filipova, L.; Fridrihsone, V.; Cabulis, U.; Berzins, A. Synthesis of nanofibrillated cellulose by combined ammonium persulphate treatment with ultrasound and mechanical processing. *Nanomaterials* **2018**, *8*, 640. [CrossRef] [PubMed]
36. Oun, A.A.; Rhim, J.W. Characterization of carboxymethyl cellulose-based nanocomposite films reinforced with oxidized nanocellulose isolated using ammonium persulfate method. *Carbohydr. Polym.* **2017**, *174*, 484–492. [CrossRef] [PubMed]
37. Cheng, M.; Qin, Z.; Liu, Y.; Qin, Y.; Li, T.; Chen, L.; Zhu, M. Efficient extraction of carboxylated spherical cellulose nanocrystals with narrow distribution through hydrolysis of lyocell fibers by using ammonium persulfate as an oxidant. *J. Mater. Chem. A* **2014**, *2*, 251–258. [CrossRef]
38. Goh, K.Y.; Ching, Y.C.; Chuah, C.H.; Abdullah, L.C.; Liou, N.S. Individualization of microfibrillated celluloses from oil palm empty fruit bunch: Comparative studies between acid hydrolysis and ammonium persulfate oxidation. *Cellulose* **2016**, *23*, 79–390.
39. Hu, Y.; Tang, L.; Lu, Q.; Wang, S.; Chen, X.; Huang, B. Preparation of cellulose nanocrystals and carboxylated cellulose nanocrystals from borer powder of bamboo. *Cellulose* **2014**, *21*, 1611–1618. [CrossRef]
40. Fortunati, E.; Benincasa, P.; Balestra, G.M.; Luzi, F.; Mazzaglia, A.; Buono, D.D.; Pugliaa, D.; Torre, L. Revalorization of barley straw and husk as precursors for cellulose nanocrystals extraction and their effect on PVA_CH nanocomposites. *Ind. Crops Prod.* **2016**, *92*, 201–217. [CrossRef]
41. Hafemann, E.; Battisti, R.; Marangoni, C.; Machado, R.A.F. Valorization of royal palm tree agroindustrial waste by isolating cellulose nanocrystals. *Carbohydr. Polym.* **2019**, *218*, 188–198. [CrossRef]
42. Luzi, F.; Puglia, D.; Sarasini, F.; Tirillò, J.; Maffei, G.; Zuorro, A.; Lavecchia, R.; Kenny, J.M.; Torre, L. Valorization and extraction of cellulose nanocrystals from North African grass: *Ampelodesmos mauritanicus* (Diss). *Carbohydr. Polym.* **2019**, *209*, 328–337. [CrossRef]
43. Yang, J.; Han, C.R.; Xu, F.; Sun, R.C. Simple approach to reinforce hydrogels with cellulose nanocrystals. *Nanoscale* **2014**, *6*, 5934–5943. [CrossRef] [PubMed]
44. Moosavinejad, S.M.; Madhoushi, M.; Vakili, M.; Rasouli, D. Evaluation of degradation in chemical compounds of wood in historical buildings using FT-IR and FT-Raman vibrational spectroscopy. *Maderas Cienc. Y Tecnol.* **2019**, *21*, 381–392. [CrossRef]
45. Schwanninger, M.; Rodrigues, J.C.; Pereira, H.; Hinterstoisser, B. Effects of short-time vibratory ball milling on the shape of FT-IR spectra of wood and cellulose. *Vib. Spectrosc.* **2004**, *36*, 23–40. [CrossRef]
46. Nascimento, S.A.; Rezende, C.A. Combined approaches to obtain cellulose nanocrystals, nanofibrils and fermentable sugars from elephant grass. *Carbohydr. Polym.* **2018**, *180*, 38–45. [CrossRef]
47. Al-Dulaimi, A.A.; Wanrosli, W.D. Isolation and characterization of nanocrystalline cellulose from totally chlorine free oil palm empty fruit bunch pulp. *J. Polym. Environ.* **2017**, *25*, 192–202. [CrossRef]
48. Yu, H.; Abdalkarim, S.Y.H.; Zhang, H.; Wang, C.; Tam, K.C. Simple process to produce high-yield cellulose nanocrystals using recyclable citric/hydrochloric acids. *ACS Sustain. Chem. Eng.* **2019**, *7*, 4912–4923. [CrossRef]
49. Oudiani, A.E.; Chaabouni, Y.; Msahli, S.; Sakli, F. Crystal transition from cellulose I to cellulose II in NaOH treated Agave americana L. fibre. *Carbohydr. Polym.* **2011**, *86*, 1221–1229. [CrossRef]
50. Ventura-Cruz, S.; Tecante, A. Extraction and characterization of cellulose nanofibers from Rose stems (*Rosa* spp.). *Carbohydr. Polym.* **2019**, *220*, 53–59. [CrossRef]
51. Suwantong, O.; Ruktanonchai, U.; Supaphol, P. Electrospun cellulose acetate fiber mats containing asiaticoside or Centella Asiatica crude extract and the release characteristics of asiaticoside. *Polymer* **2008**, *49*, 4239–4247. [CrossRef]

52. Du, C.; Liu, M.; Li, B.; Li, H.; Meng, Q.; Zhan, H. Cellulose nanocrystals prepared by persulfate one-step oxidation of bleached bagasse pulp. *BioResources* **2016**, *11*, 4017–4024. [CrossRef]
53. Montane, D.; Farriol, X.; Salvado, J.; Jollez, P.; Chornet, E. Application of steamexplosion to the fabrication and rapid vapour-phase alkaline pulping of Wheat straw. *Biomass Bioenergy* **1998**, *14*, 261–278. [CrossRef]
54. Thambiraj, S.; Ravi Shankaran, D. Preparation and physicochemical characterization of cellulose nanocrystals from industrial waste cotton. *Appl. Surf. Sci.* **2017**, *412*, 405–416. [CrossRef]
55. Ilyas, R.A.; Sapuan, S.M.; Ishak, M.R.; Zainudin, E.S. Sugar palm nanofibrillated cellulose (*Arenga pinnata* (*Wurmb.*) *Merr*): Effect of cycles on their yield, physic-chemical, morphological and thermal behavior. *Int. J. Biol. Macromol.* **2019**, *123*, 379–388. [CrossRef] [PubMed]
56. Roman, M.; Winter, W.T. Effect of sulfate groups from sulfuric acid hydrolysis on the thermal degradation behavior of bacterial cellulose. *Biomacromolecules* **2004**, *5*, 1671–1677. [CrossRef]
57. Devi, R.R.; Dhar, P.; Kalamdhad, A.; Katiyar, V. Fabrication of cellulose nanocrystals from agricultural compost. *Compos. Sci. Util.* **2015**, *23*, 104–116. [CrossRef]
58. Khanjanzadeh, H.; Behrooz, R.; Bahramifar, N.; Pinkl, S.; Gindl-Altmutter, W. Application of surface chemical functionalized cellulose nanocrystals to improve the performance of UF adhesives used in wood-based composites-MDF type. *Carbohydr. Polym.* **2019**, *206*, 11–20. [CrossRef]
59. Kasiri, N.; Fathi, M. Production of cellulose nanocrystals from pistachio shells and their application for stabilizing Pickering emulsions. *Int. J. Biol. Macromol.* **2018**, *106*, 1023–1031. [CrossRef]
60. Yang, H.; Yan, R.; Chen, H.; Lee, D.H.; Zheng, C. Characteristics of hemicellulose, cellulose and lignin pyrolysis. *Fuel* **2007**, *86*, 1781–1788. [CrossRef]
61. Jiang, F.; Hsieh, Y.L. Chemically and mechanically isolated nanocellulose and their self-assembled structures. *Carbohydr. Polym.* **2013**, *95*, 32–40. [CrossRef]
62. Isogai, A.; Saito, T.; Fukuzumi, H. TEMPO-oxidized cellulose nanofibers. *Nanoscale* **2011**, *3*, 71–85. [CrossRef]
63. Oun, A.A.; Rhim, J.W. Characterization of nanocelluloses isolated from Ushar (*Calotropis procera*) seed fiber: Effect of isolation method. *Mater. Lett.* **2016**, *168*, 146–150. [CrossRef]
64. Kaffashsaie, E.; Yousefi, H.; Nishino, T.; Matsumoto, T.; Mashkour, M.; Madhoushi, M.; Kawaguchi, H. Direct conversion of raw wood to TEMPO-oxidized cellulose nanofibers. *Carbohydr. Polym.* **2021**, *262*, 117938. [CrossRef] [PubMed]
65. Poletto, M.; Pistor, V.; Zeni, M.; Zattera, A.J. Crystalline properties and decomposition kinetics of cellulose fibers in wood pulp obtained by two pulping processes. *Polym. Degrad. Stab.* **2011**, *96*, 679–685. [CrossRef]
66. Adel, A.; El-Shafei, A.; Ibrahim, A.; Al-Shemy, M. Extraction of oxidized nanocellulose from date palm (*Phoenix dactylifera* L.) sheath fibers: Influence of CI and CII polymorphs on the properties of chitosan/bionanocomposite films. *Ind. Crops Prod.* **2018**, *124*, 155–165. [CrossRef]
67. Jiang, H.; Wu, Y.; Han, B.; Zhang, Y. Effect of oxidation time on the properties of cellulose nanocrystals from hybrid poplar residues using the ammonium persulfate. *Carbohydr. Polym.* **2017**, *174*, 291–298. [CrossRef] [PubMed]
68. Oun, A.A.; Rhim, J.W. Isolation of oxidized nanocellulose from rice straw using the ammonium persulfate method. *Cellulose* **2018**, *25*, 2143–2149. [CrossRef]
69. Oun, A.A.; Rhim, J.W. Preparation of multifunctional carboxymethyl cellulose-based films incorporated with chitin nanocrystal and grapefruit seed extract. *Int. J. Biol. Macromol.* **2020**, *152*, 1038–1046. [CrossRef]